Hydrostatic compression and high-pressure elastic constants of coesite silica

Hajime Kimizuka,[1,a)] Shigenobu Ogata,[1] and Ju Li[2]
[1]*Department of Mechanical Science and Bioengineering, Osaka University, Osaka 560-8531, Japan*
[2]*Department of Materials Science and Engineering, University of Pennsylvania, Philadelphia, Pennsylvania 19104-6272, USA*

(Received 23 August 2007; accepted 28 December 2007; published online 6 March 2008)

Using density-functional theory, we computed all the independent elastic constants of coesite, a high-pressure polymorph of silica, as functions of pressure up to 15 GPa. The results are in good agreement with experimental measurements under ambient conditions. Also, the predicted pressure-dependent elastic properties are consistent with x-ray data in the literature concerning lattice strains at high pressures. We find that coesite, like quartz, exhibits a gradual softening of a shear modulus B_{44} with increasing pressure, in contrast to the rising bulk modulus. © *2008 American Institute of Physics*. [DOI: 10.1063/1.2888558]

I. INTRODUCTION

The behavior of silica (SiO_2) under pressure is of considerable interest in geophysics and materials science. Despite its simple chemical composition, silica shows rich polymorphism at elevated pressures and temperatures. Thus the phases of silica serve as model systems for studying high-pressure and/or high-temperature phase transitions, including amorphization. Here we focus on the coesite crystal structure, originally discovered in the laboratory[1] under 3.5 GPa pressure at 750 °C. Later, coesite was also found in rocks inside the Barringer Meteorite Crater in Arizona, as well as near nuclear explosion sites, suggesting formation under impact. Coesite, like quartz and cristobalite, consists of tetrahedral units of silicon surrounded by four oxygen atoms. Of all the silica polymorphs, coesite is the highest density tetrahedrally coordinated form. It has 16 formula units of SiO_2 in a monoclinic unit cell that is nearly hexagonal.[2]

Despite its obvious importance, not much is known about the elasticity of silica under high pressure, since measurement of elastic constants is challenging under these conditions.[3] In particular elastic anisotropy, characterized by the difference in acoustic velocity in various directions, has not been systematically studied. On the other hand, a number of molecular dynamics and first-principles calculations have been performed on various high-pressure and/or -temperature silica phases, including coesite (see, for example, Refs. 4–11). However, a systematic study has not been performed on the pressure evolution of the complete set of elastic constants of coesite.

In the present article, we report the complete set of high-pressure elastic constants of coesite as determined from first-principles density-functional-theory (DFT) calculations. The data thus obtained can be compared with numerous experimental compressibility data and also the single-crystal elastic constants reported by Weidner and Carleton.[12]

II. SIMULATION TECHNIQUES

First-principles total-energy calculations under hydrostatic pressure ($\tau_{ij}=-P\delta_{ij}$, unit-cell geometries are relaxed) are performed using the Vienna *Ab-initio* Simulation Package (VASP).[13] We apply the projector-augmented-wave (PAW) method[14,15] and the Ceperley–Alder exchange-correlation potential[16] in a local-density approximation (LDA), which is parametrized by Perdew and Zunger.[17] The calculations employ the primitive cell of coesite (space group $C2/c$),[2,18,19] containing 48 atoms. A plane-wave basis set with 1400 eV kinetic energy cutoff is adopted. We also employ a $2\times2\times2$ Monkhorst–Pack[20] **k** mesh (two irreducible **k** points) for carrying out the Brillouin-zone integration, using the tetrahedron method with Blöchl correction.[21] We increase the pressure in 5 GPa increments for pressures up to 20 GPa. Forces on atoms and internal Cauchy stresses are calculated, and atomic positions and cell geometries are allowed to relax using a conjugate gradient technique until their residual forces have converged to less than 0.0005 eV/Å.

In strained crystals, the acoustic velocities correspond to the elastic stiffness coefficients or Birch coefficients (see, for example, Refs. 22 and 23). The definition of elastic stiffness coefficients $B_{ijkl}(X)$ at a finite-stress state X is given as the linear expansion coefficient of stress versus strain,[24]

$$\tau_{ij}(Y) \equiv \tau_{ij}(X) + B_{ijkl}(X)(\eta_X^Y)_{kl} + \mathcal{O}[(\eta_X^Y)^2], \tag{1}$$

where η_X^Y is the Lagrangian strain connecting states X and Y, and $\tau(X)$, $\tau(Y)$ are the Cauchy stresses of X and Y. In our calculations, a complete set of B_{ij}'s (in Voigt notation) are computed from numerical derivatives of the internal Cauchy stress with respect to strain. The crystal structure of coesite is monoclinic, which means there exist 13 independent elastic constants. The total energy and internal stress are calculated in the strained lattice for several values of the magnitude of the linear strain ϵ. Generally three values of ϵ are chosen, $\epsilon=0.005$, 0.0075, and 0.01. The unit cell is slightly deformed with every ϵ in different directions, each corresponding to a certain component of elastic constants, and then the atomic

a)Electronic mail: kimizuka@me.es.osaka-u.ac.jp.

coordinates are allowed to relax. B_{ij}'s are then obtained by fitting a line to the internal stress τ as a function of $\eta(\epsilon)$, and then taking the slope $\partial\tau/\partial\eta$.

III. RESULTS AND DISCUSSION

A. Structural variations with pressure

The lattice parameters (a, b, c, and β) and unit-cell volume (Ω) of coesite at ambient pressure are evaluated. The obtained values are a_0=7.084 (7.1366) Å, b_0 =12.327 (12.3723) Å, c_0=7.157 (7.1749) Å, β_0 =120.5° (120.33°), and Ω_0=538.5 (546.81) Å^3, where the numbers in parentheses are the experimental values[19] at room temperature. For the present method, the calculated unit-cell parameters are slightly smaller (within 0.8% for a_0, b_0, c_0 and 1.6% for volume) but fairly close to those obtained from the x-ray diffraction data.[19] The slight underestimation of the lattice constants at zero pressure is partly attributed to the LDA and partly to zero-temperature (static) calculations.

With increasing pressure from 0 to 20 GPa, the unit-cell parameters decrease continuously. Figure 1(a) shows the volume compressibility curve, along with the x-ray diffraction data from Refs. 18, 25, and 19. Note that our theoretical data obtained from the DFT calculations show good agreement with the experimental data above 20 GPa. Figure 1(b) shows the axial compressibility curves for the a, b, and c axes. The a axis is most compliant among the three axes, and the compressibility of coesite is highly anisotropic in the a-c plane. This behavior is due to the aligned silicate chains that run parallel to c.[18] The chains are relatively stiff along their lengths, but the structure is relatively flexible in the a direction, largely inclined from the chains. Our theoretical data are found to agree well with the experimental data all for a, b, and c, as indicated in Fig. 1(b). This result suggests that our calculations have the ability to satisfactorily reproduce the anisotropic compression behavior of coesite.

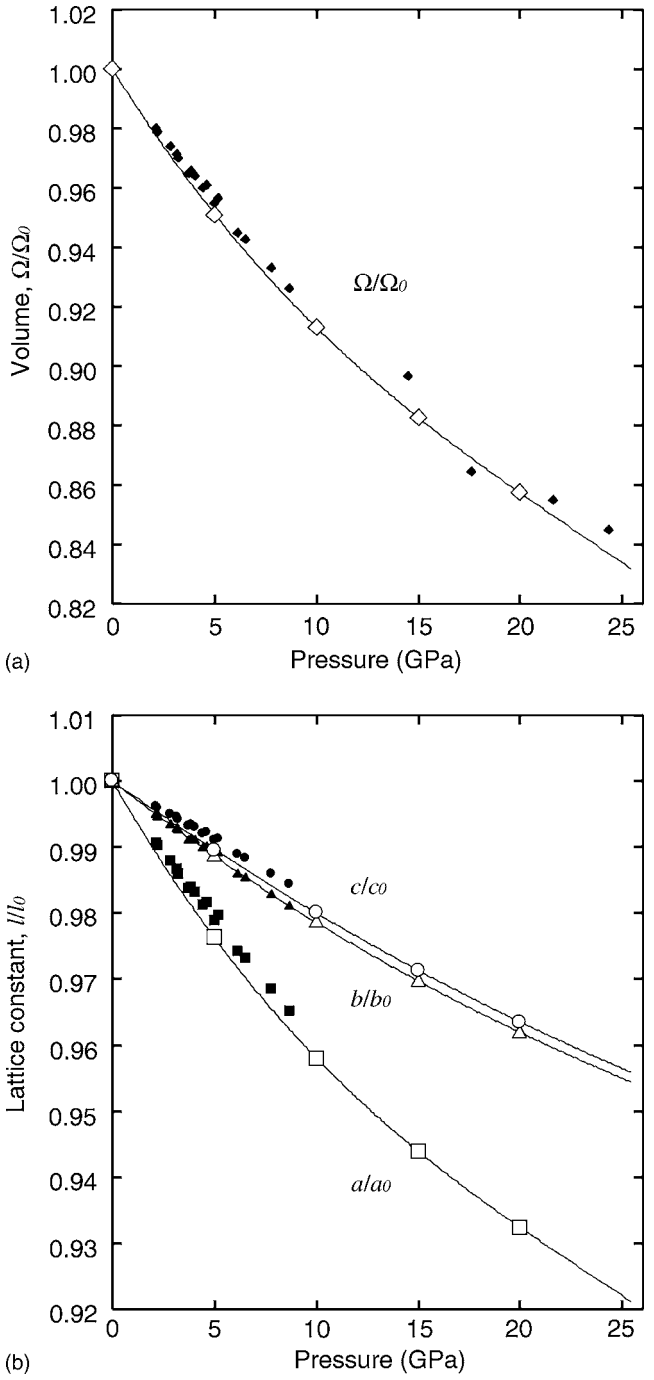

FIG. 1. Pressure evolution of the (a) unit-cell volume and (b) lattice constants of coesite. (a) The open diamonds represent data from the DFT calculations. The x-ray diffraction data (solid symbols) are from Refs. 18, 25, and 19. (b) The open squares, triangles, and circles represent normalized lattice lengths a/a_0, b/b_0, and c/c_0 obtained from the DFT calculations, respectively. The x-ray diffraction data (solid symbols) are from Refs. 18 and 19.

B. Elastic constants

The elastic stiffness coefficients (B_{ij}) of coesite are evaluated under pressure from 0 to 15 GPa using the DFT calculations (Table I). We have included the experimental values[12] at ambient pressure for comparison, which were determined from Brillouin scattering measurements. Whereas B_{11}, B_{22}, and B_{33} are within 12–15% off the experimental values, the deviation for B_{44}, B_{12}, and B_{13} is larger, around 24–33%. This large deviation may be understood from the fact that these three elastic constants have relatively low magnitudes. The rank order of the 13 elastic stiffness coefficients is largely preserved.

Figure 2 displays the pressure evolution of the B_{ij}'s. A similar monotonous pressure dependence is observed, however their magnitudes are quite different. With increasing pressure up to 15 GPa, the B_{11}, B_{22}, and B_{33} values increase significantly and their pressure dependence is nonlinear, whereas B_{55} and B_{66} change little and are almost constant in this pressure range. In particular, it is noteworthy that B_{44} manifests negative pressure slope. This behavior of the elastic constants indicates the possibility that the high-pressure phase transition in coesite will be driven by softening of the shear modulus B_{44}, and the shear instability occurs at high pressure.

The bulk modulus (K) of monoclinic crystals depends on a combination of elastic compliance constants S_{ij}, the inverse of the B_{ij} matrix,[26]

$$K^{-1} = S_{11} + S_{22} + S_{33} + 2(S_{12} + S_{13} + S_{23}). \quad (2)$$

TABLE I. Calculated values for elastic stiffness coefficients (B_{ij} in GPa), bulk modulus (K in GPa), and the ratio of linear compressibilities (k_a/k_b and k_c/k_b) of coesite, together with experimental values.

	$P=0$ (GPa)		5 (GPa)	10 (GPa)	15 (GPa)
	Expt.[a]	Calc.	Calc.	Calc.	Calc.
B_{11}	160.8	142.0	153.3	185.4	212.4
B_{22}	230.4	199.6	240.8	263.6	290.4
B_{33}	231.6	197.5	214.6	241.7	268.7
B_{44}	67.8	45.1	40.5	27.4	21.9
B_{55}	73.3	70.2	72.1	75.0	78.0
B_{66}	58.8	58.7	58.1	54.7	54.8
B_{12}	82.1	57.3	69.8	87.0	102.8
B_{13}	102.9	78.1	85.5	109.8	127.1
B_{15}	−36.2	−29.8	−30.2	−24.5	−21.6
B_{23}	35.6	39.0	58.8	73.5	92.3
B_{25}	2.6	13.4	16.1	14.1	14.9
B_{35}	−39.3	−33.0	−28.6	−20.1	−15.9
B_{46}	9.9	10.2	10.3	4.2	5.3
K	109.1	93.1	108.0	133.4	154.8
k_a/k_b	1.60	1.71	2.34	1.66	1.54
k_c/k_b	1.11	1.10	1.30	1.03	0.99

[a]Reference 12.

According to Eq. (2), the K values derived from the B_{ij}'s (via the S_{ij}'s) at various pressures are also tabulated in Table I. By another way, we can determine K from fitting a polynomial to the pressure dependence of $\ln \Omega$, based on Fig. 1(a). With the best-fit coefficients of a third-order polynomial, K $(\equiv -dP/d \ln \Omega)$ is calculated as a function of P. The obtained values are 89.6, 111.2, 135.2, 159.7, and 183.9 GPa at pressures of 0, 5, 10, 15, and 20 GPa, respectively. Figure 3 shows the pressure evolution of the bulk modulus obtained in the analysis. The numerical derivative of pressure with respect to volume $(-dP/d \ln \Omega)$ is shown as a solid curve as a function of P, based on the theoretical volume compressibility data, also along with the x-ray experimental data (open circles) from Refs. 18, 25, and 19. It is noteworthy that the K values derived from our B_{ij}'s are consistent with these volume compressibility data.

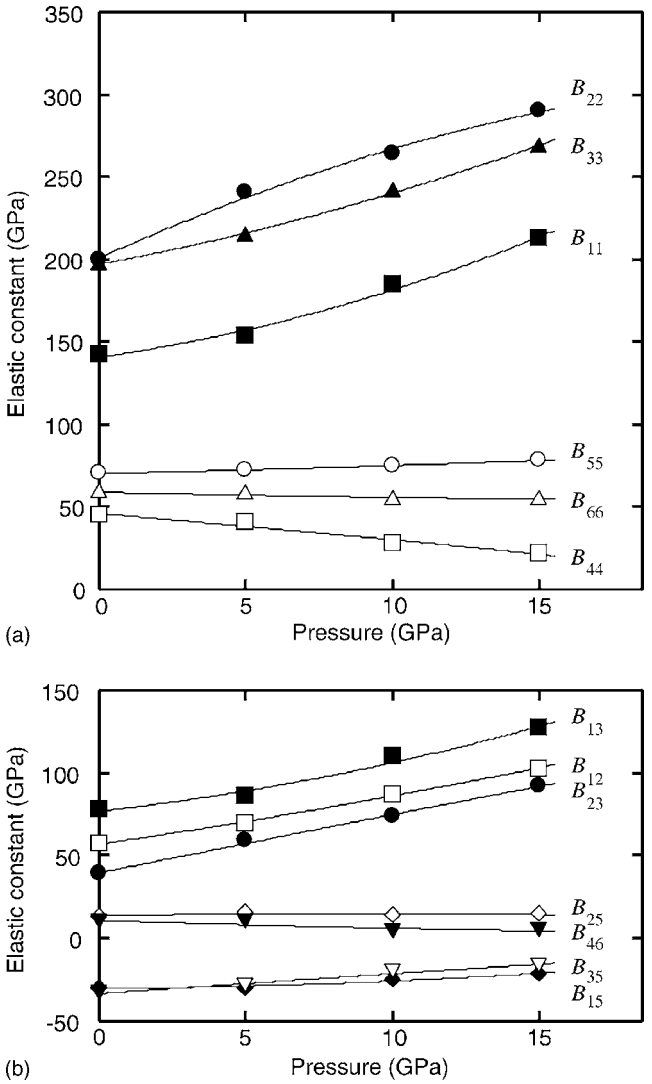

FIG. 2. Pressure evolution of the elastic stiffness coefficients of coesite. (a) Diagonal components; B_{11} (solid square), B_{22} (solid circle), B_{33} (solid triangle), B_{44} (open square), B_{55} (open circle), and B_{66} (open triangle). (b) Off-diagonal components; B_{12} (open square), B_{13} (solid square), B_{15} (solid diamond), B_{23} (solid circle), B_{25} (open diamond), B_{35} (open inverted triangle), and B_{46} (solid inverted triangle).

C. Linear compressibility

The pressure dependence of the lattice parameter is also related to a combination of elastic constants, and thus we can make use of the linear compressibility k to check the validity of the calculated B_{ij}'s. In monoclinic crystal, the axial compressibilities k_a, k_b, and k_c are of the form[26]

$$k_a = -d \ln(a)/dP = S_{11} + S_{12} + S_{13},$$

$$k_b = -d \ln(b)/dP = S_{12} + S_{22} + S_{23},$$

$$k_c = -d \ln(c)/dP = S_{13} + S_{23} + S_{33}. \quad (3)$$

Here the ratios k_a/k_b and k_c/k_b reflect the anisotropy of the linear compressibility. On the other hand, we can determine k_a/k_b and k_c/k_b by fitting a polynomial to the evolution of $\ln(a)$ and $\ln(c)$ with respect to $\ln(b)$ at various pressures. Thus we could examine the consistency between the k ratios derived from the strained lattice parameters and those derived from the calculated B_{ij} values.

Figure 4 displays the relations among the three axial compressibilities for coesite, along with the diffraction data from Refs. 18 and 19. As clearly shown in Fig. 4, the logarithms of a and c change linearly with $\ln(b/b_0)$ both for the DFT and experimental data, and the slopes of their least-squares fits are almost the same: 1.87 and 0.948 for the DFT data on $\ln(a/a_0)$ and $\ln(c/c_0)$, and 1.85 and 0.795 for the experimental data on $\ln(a/a_0)$ and $\ln(c/c_0)$, respectively.

Our predicted B_{ij}'s for coesite as listed in Table I yield the ratio of k values at various pressures. At ambient pressure, the k_a/k_b and k_c/k_b values derived from the DFT data and the experimental data[12] agree well with one another. At above 5 GPa, the k_a/k_b values (ranging from 1.54 to 2.30) and k_c/k_b values (ranging from 0.99 to 1.30) apparently coincide with the above k ratios over the pressure range up to

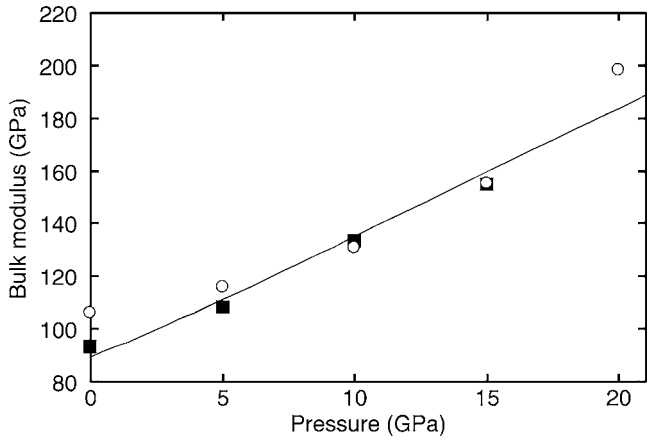

FIG. 3. Pressure evolution of the bulk modulus of coesite. The DFT values derived from Eq. (2) are indicated as solid squares. Solid curve represents the numerical derivative, $-dP/d\ln\Omega$, based on the DFT *P-V* curve. For comparison, the experimental $-dP/d\ln\Omega$ values are plotted as open circles, based on the x-ray diffraction data.[18,25,19]

15 GPa. This suggests that the present B_{ij}'s are consistent with the compressibility behavior, both for the experimental and DFT data.

IV. CONCLUSIONS

We have obtained the high-pressure elastic constants of coesite via first-principles density-functional-theory calculations. Our results are consistent with not only the elastic constants obtained from Brillouin scattering measurements at ambient pressure, but also the x-ray diffraction data concerning the volume and axial compressibilities in high-pressure experiments. The present calculations provide insight into the elastic behavior of coesite at high pressure, and help us better understand the physics of solid silica.

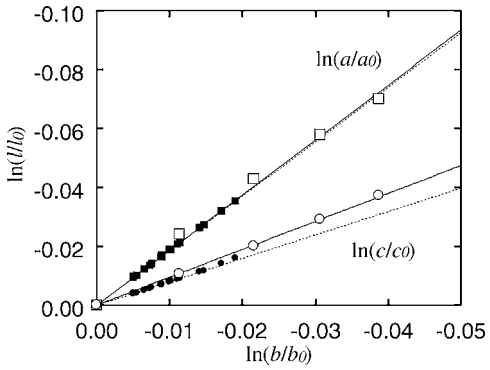

FIG. 4. Plot of logarithmic lattice lengths as a function of $\ln(b/b_0)$ for coesite. Open squares and open circles represent the DFT data for $\ln(a/a_0)$ and $\ln(c/c_0)$ in this study, and the solid lines are the best fit with the slope 1.87 and 0.948, respectively. The x-ray diffraction data (small solid symbols) are from Refs. 18 and 19 and the dotted lines are the best fit with the slope 1.85 and 0.795 for $\ln(a/a_0)$ and $\ln(c/c_0)$, respectively.

ACKNOWLEDGMENTS

The authors would like to thank Yoji Shibutani and Hideo Kaburaki for useful discussion. Work of S.O. is supported by the Next Generation Supercomputer Project, Nanoscience Program, MEXT, Japan. Work of J.L. is supported by NSF DMR-0502711, DOE DE-FG02-06ER46330, USAFOSR, ONR N00014-05-1-0504, and Ohio Supercomputer Center.

[1] L. Coes, Science **118**, 131 (1953).
[2] G. V. Gibbs, C. T. Prewitt, and K. J. Baldwin, Z. Kristallogr. **145**, 108 (1977).
[3] A. Polian, J. Raman Spectrosc. **34**, 633 (2003).
[4] J. R. Chelikowsky, H. E. King, Jr., N. Troullier, J. L. Martins, and J. Glinnemann, Phys. Rev. Lett. **65**, 3309 (1990).
[5] J. S. Tse and D. D. Klug, Phys. Rev. Lett. **67**, 3559 (1991).
[6] N. Binggeli and J. R. Chelikowsky, Phys. Rev. Lett. **69**, 2220 (1992);N. Binggeli and J. R. Chelikowsky, *ibid.* **71**, 2675 (1993).
[7] D. M. Teter, R. J. Hemley, G. Kresse, and J. Hafner, Phys. Rev. Lett. **80**, 2145 (1998).
[8] H. Kimizuka, H. Kaburaki, and Y. Kogure, Phys. Rev. Lett. **84**, 5548 (2000).
[9] D. W. Dean, R. M. Wentzcovitch, N. Keskar, J. R. Chelikowsky, and N. Binggeli, Phys. Rev. B **61**, 3303 (2000).
[10] H. Kimizuka, H. Kaburaki, and Y. Kogure, Phys. Rev. B **67**, 024105 (2003).
[11] H. Kimizuka, S. Ogata, J. Li, and Y. Shibutani, Phys. Rev. B **75**, 054109 (2007).
[12] D. J. Weidner and H. R. Carleton, J. Geophys. Res. **82**, 1334 (1977).
[13] G. Kresse and J. Furthmüller, Phys. Rev. B **54**, 11169 (1996).
[14] P. E. Blöchl, Phys. Rev. B **50**, 17953 (1994).
[15] G. Kresse and D. Joubert, Phys. Rev. B **59**, 1758 (1999).
[16] D. M. Ceperley and B. J. Alder, Phys. Rev. Lett. **45**, 566 (1980).
[17] J. P. Perdew and A. Zunger, Phys. Rev. B **23**, 5048 (1981).
[18] L. Levien and C. T. Prewitt, Am. Mineral. **66**, 324 (1981).
[19] R. J. Angel, C. S. J. Shaw, and G. V. Gibbs, Phys. Chem. Miner. **30**, 167 (2003).
[20] H. J. Monkhorst and J. D. Pack, Phys. Rev. B **13**, 5188 (1976).
[21] P. E. Blöchl, O. Jepsen, and O. K. Andersen, Phys. Rev. B **49**, 16223 (1994).
[22] D. C. Wallace, Rev. Mod. Phys. **37**, 57 (1965).
[23] T. H. K. Barron and M. L. Klein, Proc. Phys. Soc. **85**, 523 (1965).
[24] J. Li, Ph.D. thesis, MIT (2000).
[25] R. J. Hemley, A. P. Jephcoat, H. K. Mao, L. C. Ming, and M. H. Manghnani, Nature (London) **334**, 52 (1988).
[26] J. F. Nye, *Physical Properties of Crystals: Their Representation by Tensors and Matrices* (Clarendon, Oxford, 1985).